Neutron and X-ray tomography at Necsa

by F.C. de Beer*

Synopsis

The utilization of computer assisted tomography (CT or CAT-scan) as general non-destructive examination (NDE) technique and as research tool for scientists in South Africa, is limited due to the relative unavailability or nonexistence of such specialized analytical equipment. Many medical hospitals are equipped with X-ray CT scanners for the diagnostic examination of patients but do not easily allow paleontologist or other scientist to utilize their very expensive equipment.

As from 2003, Necsa hosts the South African Neutron Radiography (SANRAD) and tomography facility where neutrons from the SAFARI-1 nuclear research reactor and their penetrating power as well as X-rays as a complementing tool, are utilized in many R&D applications. This facility is being made available to HEI and specifically utilized by postgraduate students as part of their studies and/or by industry on an ad hoc commercial basis.

The capability of these radiation imaging facilities at Necsa will be demonstrated in areas such as paleontology, geosciences and specifically the physical properties of rock and the distribution of minerals in borehole cores, petrophysics to predict the percentage tar/oil/water content within sandstone samples and others.

The penetration capability of neutrons through specimens with a matrix of high atomic number (dense materials) and their ability to be attenuated by low atomic number material (light density) makes neutron imaging complementary to X-ray imaging. The capability of X-ray and gamma radiation for relatively easy penetration through specimens of low atomic number allows for viewing of imbedded high atomic number materials and density variation. X-ray micro focus radiography is capable of resolving objects of micro scale size that are micro distances apart whereas X-ray phase contrast radiography utilizes the wave properties of the electromagnetic spectrum of X-rays to clearly define edges of the specimen under investigation.

Many applications with neutrons as imaging probe are successfully applied at several facilities across the globe such as at NIST in USA, Neutra at PSI in Switzerland, and ANTARES at FRM2 in Germany, etc, are documented[4–9], through world conferences on neutron radiography, for example. This is achieved through very well thought through and implemented instrumentation from the production of neutrons to their detection and interpretation of the images. The need arose at Necsa to upgrade the current facility from 42-year-old technology, which was successfully applied in neutron imaging over the past 10 years, to state-of-the-art technology found at European facilities. This initiative started under the auspices of an IAEA-TC programme for the period 2007–2010.

Experimental facilites

Neutrons are sourced from the SAFARI-1 nuclear research reactor operated by Necsa. Necsa is located at Pelindaba in the Northwest Province of South Africa, which is 30 km west of Pretoria. The South African Neutron Radiography (SANRAD) facility is located on the beam port floor of the SAFARI-1 nuclear research reactor hall and sources neutrons from beam port No. 2. The facility has neighbouring facilities, i.e. a small angle neutron scattering (SANS) facility (beam port No. 1) and a neutron diffraction (NDIFF) facility (beam port No. 5), as shown in Figure 1.

Neutron beam source

Neutrons are produced in the SAFARI-1 reactor core through controlled fission of enriched ^{235}U nuclear fuel in 4π. The fast neutron beam emanating from the fission process is moderated into thermal neutrons by the water surrounding the reactor core. From the reactor core, a beam tube directs the neutron beam through a collimation (beam shaping) system to the radiography experimental facility on the beam port floor of the reactor.

The collimation system consists of a laminated structure built up from sections of Fe (iron) and PE (polyethylene). The function of the collimator is to attenuate scattered neutrons and let neutrons travel in one direction towards the detector plane. A bismuth crystal located in the beam path eliminates most of the gamma rays emanating from the fission reaction as well as the prompt gamma rays produced from the scattered neutrons. This renders the neutron beam 93%

* *Necsa (South African Nuclear Energy Corporation Ltd).*

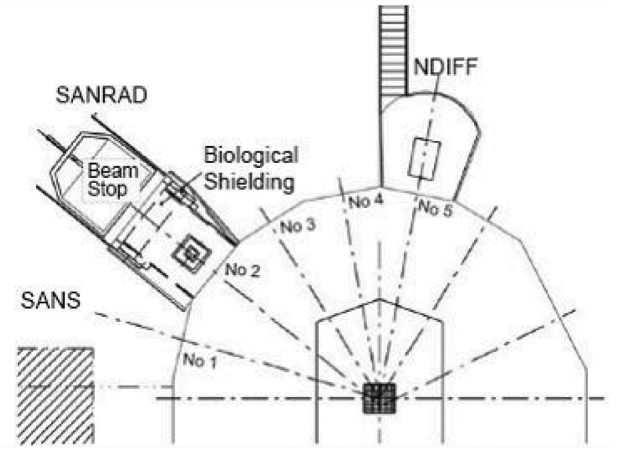

Figure 1— Schematic layout of location of SANRAD on the beam port floor of the SAFARI-1 research reactor

thermal. Specifications and the characteristics of the neutron beam and those of the collimation system are summarized in Table I.

At 20 MW reactor power and using a 21 mm interior pinhole diameter neutron passage in the collimator, a neutron flux of 1.2×10^7 n.cm^{-2}.s^{-1} is delivered at the object position in the centre of beam. Two beam shutters, one in the interior of the collimator that controls the image quality and an exterior main beam shutter that controls the exposure to radiation, form part of the collimator set-up.

The exterior beam shutter as the main beam shutter has a 300 mm diameter and the interior has three diameters (D) of 6, 10 and 21 mm to choose from, depending on the required neutron beam flux, needed dynamic range of the radiographs and spatial resolution.

Table I

Specifications and the characteristics of the neutron beam and collimation system [10]

Distance (L) for the aperture to the detection system		3000 mm
Beam diameter at outlet of collimator		300 mm
Neutron flux at object in center of beam (n.cm^{-2}.s^{-1}) at 20 MW reactor power & pinhole (D) = 21 mm		1.2×10^7
Separate pinhole apertures:		Collimation ratio L/D:
	D = 6 mm	500
	D = 10 mm	300
	D = 21 mm	143
Beam divergence at:	D = 6 mm	0.9°
	D = 10 mm	1.5°
	D = 21 mm	3.2°

Table II

Specifications and character of the x-ray beam[10]

Distance (L) for the aperture to the detection system	800 mm
Cone beam diameter at scintillator	728 mm
Focal spot D:	Collimation ratio L/D:
D = 1 mm	800
D = 3 mm	267
X-ray tube voltage range	0–100 kV
Beam divergence	40°

X-ray beam source

A 100 kV X-ray tube can be installed at the exit of the collimator to replace the neutron beam delivery with X-rays. The power supply and the control panel are located in the laboratory control area, outside the facility's containment. A change in voltage and electrical current is observed on the image produced on the frame grabber computer. Characteristics of the X-ray beam and the imaging properties are summarized in Table II[10].

SANRAD facility containment

The SANRAD facility consists of a radiation containment component, shown in Figure 2, and an experimental control area. The containment is where a sample is exposed to neutron or X-ray radiation and shields the surrounding area from penetrating neutron and X-ray radiation beams. The imaging system for radiography is located inside the containment. An experimental control area is where stage rotations and image acquisition are controlled. This is also where the pinhole size is selected and main shutter is opened and closed. There are two Pentium-4 computers in place to assist with operations including image manipulation, data acquisition and reconstruction of 3-D images.

The containment serves as an enclosed radiological shielding with ($200 \times 200 \times 200$) cm^3 internal dimensions. The reactor core concrete structure forms one of the vertical sides, while the other three (including the roof) consists of 45 cm thick high density concrete covered on the inside with layers of 2 cm thick wax tiles containing 5% boron by mass, covered by 2 cm thick polyethylene sheet. Part of the concrete roofing directly above the sample area is removable to accommodate samples longer than 200 cm. The outer area of the side walls of the containment is covered with 5 cm lead (Pb), for shielding against secondary gamma rays emerging from neutron interaction with the sample and concrete shielding. The side of the containment opposite to beam entry is used as the entrance and beam stop. It is a 150 cm thick sandwich-like structure of 0.5 cm steel layer housing filled with concrete and PE layers. It is driven backwards and forwards by a motor. The front surface of the beam stop is covered with a 4 cm layer of wax containing 5% boron by mass to thermalize the fast neutron component of the beam and captures the thermal neutron beam.

SANRAD tomography set-up and capabilities

Shown in Figure 3 is the current layout of the South African Neutron Radiography (SANRAD) facility used in industrial tomography investigations at Necsa. This facility is used to obtain both radiographs and tomograms based on X-rays (100 kV X-ray tube) and thermal neutron.

The sample (non-human) is placed on a rotary table in between the imaging system and radiation source. The turntable is stepwise rotated and moved across the scintillator screen using TOMOCONTROL PC and LabView software interface. With radiation incident on the sample and partly transmitted through the sample, radiographs can be obtained

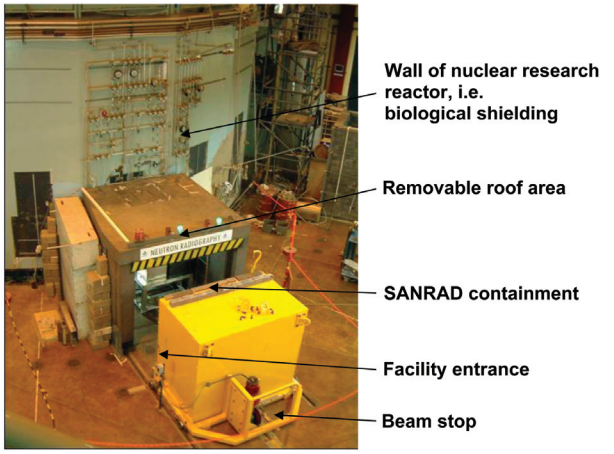

Figure 2—SANRAD facility containment

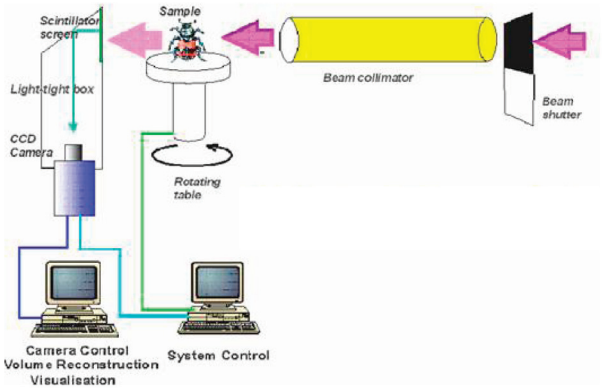

Figure 3—A schematic diagram of the layout of the Radiography and Tomography Facility at Necsa[10]

at each step angle of the rotation through an Andor CCD Peltier cooled camera and its image acquisition software package[11].

The process of detecting of neutron penetrating radiation is made possible through a scintillator screen, charge coupled device (CCD) camera, and computer with a frame grabber.

The cone-beam, parallel beam- and fan beam reconstruction ability Octopus[2] or IDL[12] is utilized to reconstruct the samples through the Fourier backprojection algorithm into axial 3D slices. Visualization of volumetric data sets (combination of the axial slices) is achieved through VGStudio(Max)[3] and IPPLUS[13] software packages.

Scintillator screens used for neutron and X-ray detection are (^{6}LiF/ZnS: Cu, Al, Au) and Gd_2O_2S respectively[14]. A front surface-coated mirror mounted at 45° vertical to the incident beam reflects the photon image from the scintillator screen through a lens on the CCD camera, thus protecting the CCD camera from being directly exposed to incident radiation.

A variety of lenses are employed, which are focused onto the scintillator screen in order to improve the image spatial resolution, especially for small samples. Different lenses vary resolution of the image and vary the field of view (FOV) on the scintillator screen. Table III presents the spatial resolution obtained with various SMC-Pentax lenses.

Images are captured by a Peltier-cooled CCD camera. Its specification is an Andor type with 1024 × 1024 pixel array and 16-bit image output device at $2_{\mu s/pixel}$. The Peltier-cooled CCD camera has an image acquisition rate of 1.2 s but can be adjusted to produce a radiograph at full dynamic range. It captures photo images reflected from the scintillator screen through the Pentax lens. The camera chip can be cooled to –75°C to minimize dark current to less than 0.05 electrons/pixels but it is normally utilized at –45°C. Dark current incorporates gray value errors due to the contribution of electrons from the electronics into electron wells for gray value determination.

The translation table, shown in Figure 3, is used for the horizontal rotation of the sample to enable taking images, at different angles, with the imaging system for different projections that are used for 3-D tomographic reconstructions. The platform on which the sample is put is available in different sizes to accommodate different sized objects. The movement is available in four directions, i.e. x-sideways, y-backwards and forwards, z-upwards and downwards, and r-horizontal rotations relative to the scintillator screen. A stepper motor controls the horizontal rotation of the sample to enable acquisition of radiographs at sample rotations between 0° to 360°, and the X-translation across the detector is for the positioning of the sample within the field of view. Y- and Z- translations are performed manually to position the sample at the appropriate distance and horizontal level in front of the detector.

Table III

Specifications of various SMC-Pentax lenses[10]

Pentax lens type	Field of view (FOV) (mm^2)	Spatial resolution (pixels/mm)
A 50 mm/F1.2	250 × 250	3.8
FA 100 mm/F2.8	130 × 130	7.7
FA 135 mm/F2.8	100× 100	10.3

Facility upgrade

SANRAD (neutron radiography) facility

The need for upgrade of the SANRAD facility is as a result of the current inadequate state of shielding, the corrosion of the collimation system, inhomogeneous beam profile and relatively low flux. This upgrade is also because of the demand of a multifunctional system that offers fast neutron, thermal neutron, gamma ray, phase contrast and dynamic radiography.

The layout of the current SANRAD facility is schematically shown in Figure 4, with the shielding and experimental chamber close to the reactor wall; the planned facility layout is shown in Figure 5 with an extended flight tube and larger experimental chamber surrounded by complete enclosed heavy concrete shielding with thickness of 80 cm towards the reactor and 60 cm towards the rear of the facility respectively.

Through MCNP simulation the beam profile at the detector plane is determined prior to manufacturing and

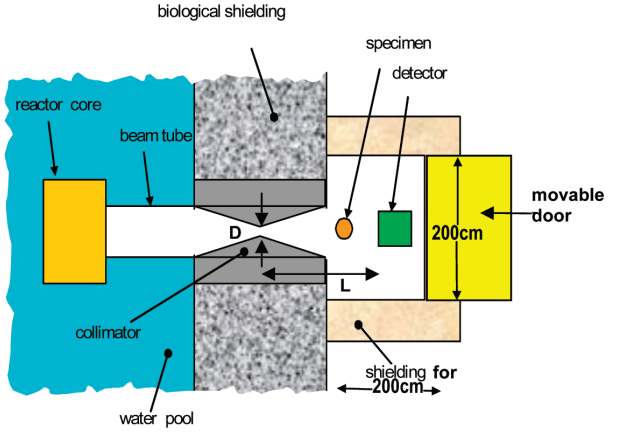

Figure 4—Current layout of the SANRAD facility (schematic overview)

installation and is compared with the old facility. Currently, the beam profile is inhomogeneous and is shown in Figure 6. After installation of the new collimator, a flat beam profile at the detection plane is being envisaged, as shown in Figure 7, with a subsequent higher dynamic range output than the current collimator.

Hexray (high energy X-ray), Mixray (micro-focus X-ray) and Gamray (gamma ray) facilities

Due to higher demand for analytical imaging techniques based on radiation penetration, the need for establishment of the high energy X-ray radiography and tomography facility, microfocus X-ray and gamma ray facility are planned. These facilities will be separate from the SANRAD facility. It is planned to subdivide a hall to house high energy X-ray-, gamma ray radiography and tomography, X-ray phase contrast and X-ray micro-focus systems, as independently shielded facilities.

Developments of the relatively high energy X-ray radiography and tomography system are in progress. This include the purchasing of a high energy X-ray tube, design and manufacturing of the X-ray shielding; and design and purchase of components of the electronic detection system,

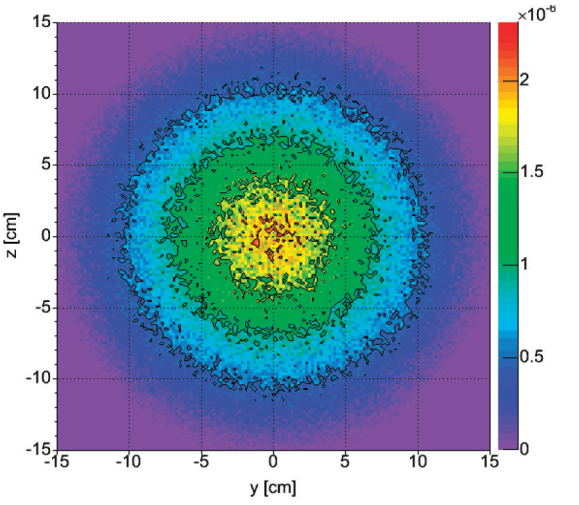

Figure 6—Neutron beam flux at the detector plane resulting from the current collimation system

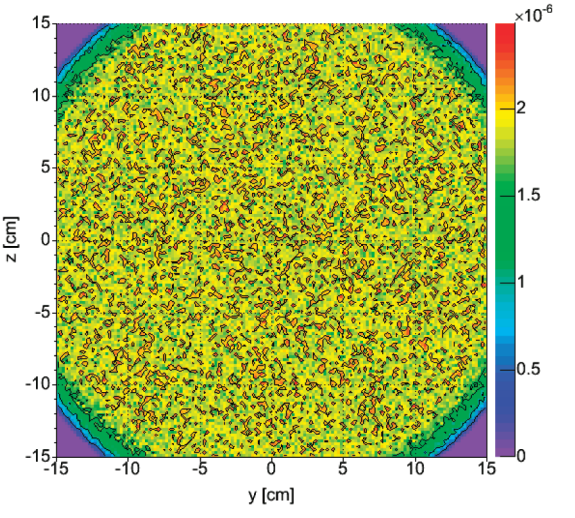

Figure 7—Neutron beam flux at the detector plane simulated for the new facility

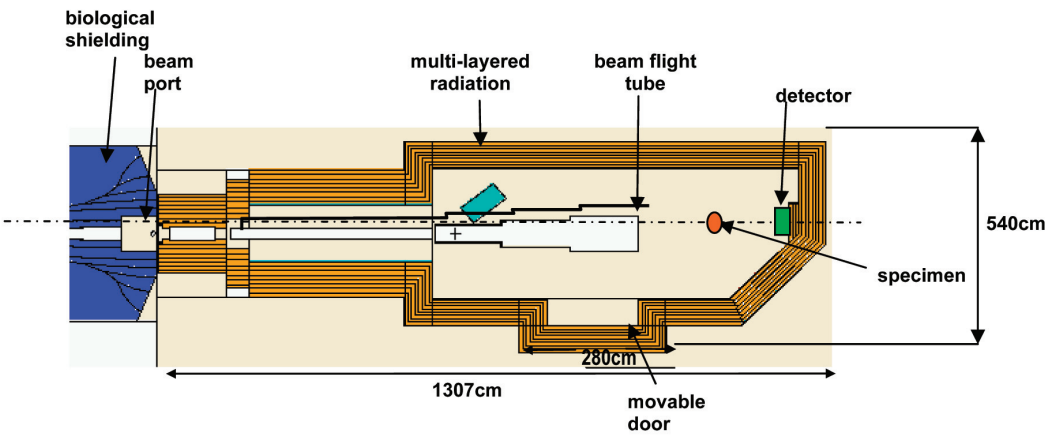

Figure 5—Planned envisaged layout of the SANRAD facility (schematic overview) generated through MCNP simulation software

specimen stage and translation table and source holder equipment. Furthermore, the certification of the building to host ionizing radiation for analytical purposes is in progress.

The establishment of a micro-focus X-ray facility gains momentum as an old system, currently located at the CSIR, could be refurbished and relocated at Necsa. This system will have the capability of 1–5 micron spatial resolution with endless applications which include biosciences, and composite aircraft industry in collaboration with the CSIR.

The gamma-ray facility could be established soon as Necsa is involved in a consortium with two industrial companies for the establishment of such a facility to cater for the needs of the geosciences in mineral exploration. The proposed infrastructure entails a 450 kV high energy X-ray source with a possible X-ray linear array as detector.

Applications

Some of the most recent applications at the SANRAD facility to different disciplines are described in the following paragraphs:

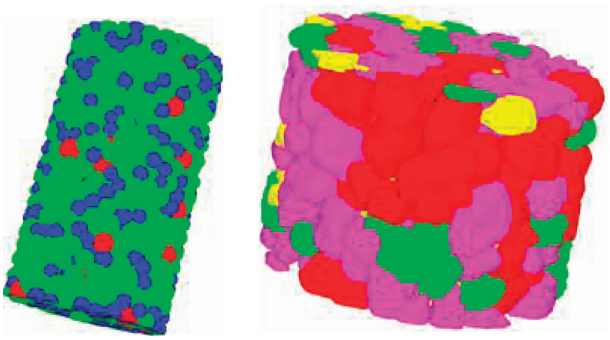

Figure 8—3-D neutron tomograms of porous media: spherical beads (left), sandstone fragments (right); different colours depict different particle size

Quantification of porous media:

Porous media characterization is important for civil and petro-physical fraternities because fluid flow behaviour within porous media is influenced by parameters such as porosity, pore size, pore interconnectivity, aggregate size and -shape. The determined the parameters obtained through neutron imaging can be used to calculate permeability of porous media.

Quantifying beads and sandstone samples for the characterization of the porous media with 50 micron resolution is being obtained with the current X-ray system compared to the 100 microns offered by neutrons. In this application, resolving between two constituencies is crucial for the determination of the true shape and size of constituencies that are closely packed. The tomography reconstructions of beads and sandstone in Figure 8 show the size and shape of particles that affect the porosity property.

Geological application:

Figures 9 (a), (b) and (c) are neutron 3-D and 2-D images (slices) showing the distribution and location of orthopyroxene (green) and clinopyroxene (red) within the geological drill core (diameter = 2.4 cm, height = 8 cm). The capability of tomography to present the distribution and location of minerals in different aspects is an important feature shown in these images.

This was achieved using the penetration capability of thermal neutrons through the palioglace matrix (thermal neutron linear attenuation coefficient to be 0.03 cm^{-1} as apposed to 3,01 cm^{-1} for the X-rays) as well as the difference in thermal neutron linear attenuation coefficients of orthopyroxene (0.41 cm^{-1}) and clinopyroxene (0.29 cm^{-1}). If the sample consists of different minerals that attenuate neutrons differently, they can be distinguished within the material as long as neutrons are being transmitted through the sample.

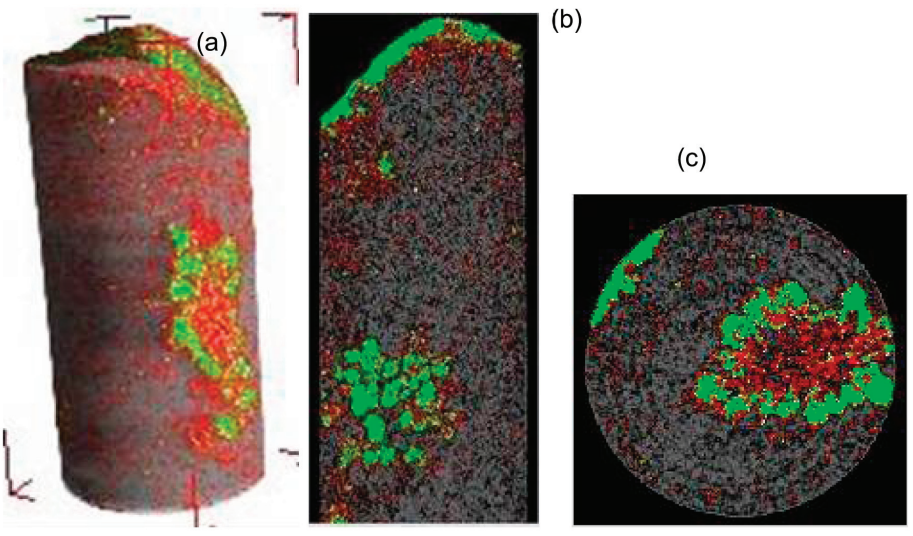

Figure 9—(a) 3-D image of geological core revealing distribution and location of orthopyroxene (green) and clinopyroxene (red) within the geological core. (b) and (c) views that expose orthopyroxene (green) and clinopyroxene embedded within the geological core after frontal and axial cuts respectively into the tomogram

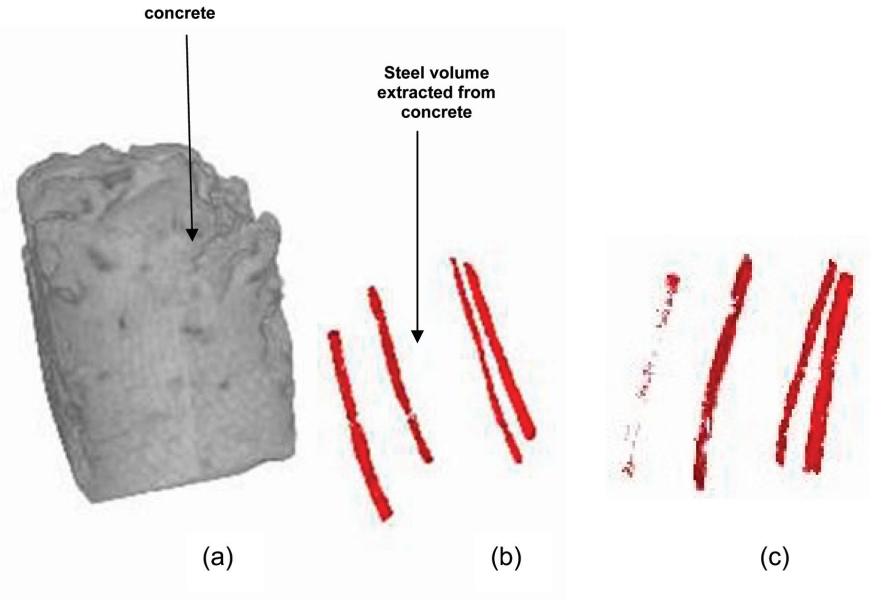

Figure 10—(a) 3-D tomogram of a steel reinforced concrete sample. (b) Steel elements, before submersion to NaCl solution, extracted from within the 3-D image of concrete using software. (c) Steel elements, after submersion to NaCl solution, extracted from within the 3-D image of concrete using analytical software

Steel degradation within concrete : civil engineering application:

Neutron tomography is useful in studies of the integrity of steel reinforced concrete. This technique has been used to image the shape, location and size (volume) of the steel elements embedded in a laboratory concrete sample (4.5 cm × 4.5 cm × 6.0 cm) and its corrosion rate without physically destroying the concrete sample. This was achieved by segmenting plain concrete from steel plates embedded in concrete using the considerable difference in their thermal neutron mass attenuation coefficient. The theoretical thermal neutron mass attenuation coefficient values of concrete and that of steel are $0.15 cm^2.g^{-1}$ and $1.16 cm^2.g^{-1}$ respectively. Figures 10 (a) and (b) show the reconstructed 3-D image of steel reinforced concrete and extracted steel elements before submersion in the 20%wtNaCl solution respectively. After eight weeks submersion in the 20%wt NaCl solution the steel volume was 11% reduced as shown in Figure 10 (c).

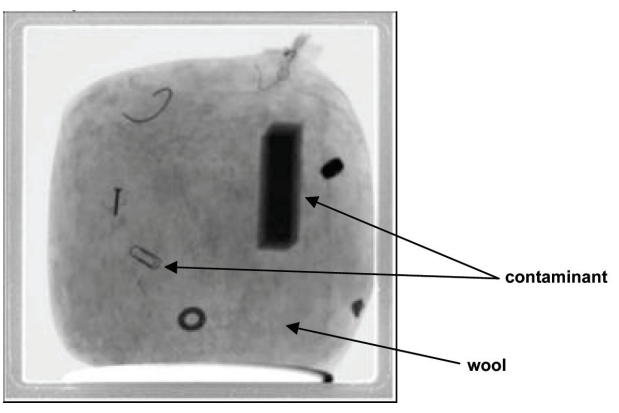

Figure 11—An x-ray radiograph of a wool phantom with contaminants embedded within the wool phantom

Quality control: embedded contamination in wool

An X-ray radiograph of a wool phantom (25 cm x 25 cm x 25 cm) with contaminants (concrete, metallic washer, metallic screw, metallic paper clip, metallic nut and string of nylon) embedded within the wool phantom is shown in Figure 11. Radiography clearly reveals these contaminants from within the wool phantom, and this viewing of the contaminants within wool is possible because wool consists of light nuclides that are generally transparent to X-rays and contaminants are either heavier nuclides or lighter nuclides of higher density.

Mechanical engineering

Shown in Figures 12 (a), (b), (c), and (d) is a helicopter engine lubricator responsible for lubrication using oil through a small 2 mm diameter pipe. It is important that this critical component of this lubricator remains unblocked for proper functioning. Figure 12 (a) shows the photograph of the engine lubricator; Figures 12 (b), (c) and (d) present the neutron tomograms of this component. Neutrons could penetrate the tungsten and provide a 3-D model of the engine component. Neutron tomography could, after reconstruction and visual analysis of the engine lubricator, reveal the blockage, its location and size without physically cutting the lubricator and welding again. The cutting and welding practice is not desired because it might introduce blockages as well as introduce structural weakness.

This 3-D image of the engine lubricator was made possible through the penetrating nature of thermal neutrons through material of high atomic number-steel- and neutrons' general better attenuation by low atomic number materials (hydrogen in oil or water); hence by the considerable difference in thermal neutron mass attenuation coefficients of stainless steel, which is iron ($0.15 cm\ 2.g^{-1}$) alloys, and oil ($3.52 cm\ 2.g^{-1}$). The 3-D image also serves as the reverse

Neutron and X-ray tomography at Necsa

Figure 12—(a) A photograph of a stainless steel helicopter engine lubricator

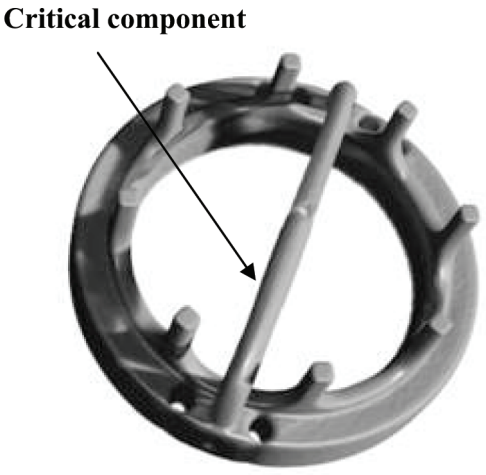

Figure 12—(c) A neutron tomogram of the critical component of a helicopter engine lubricator

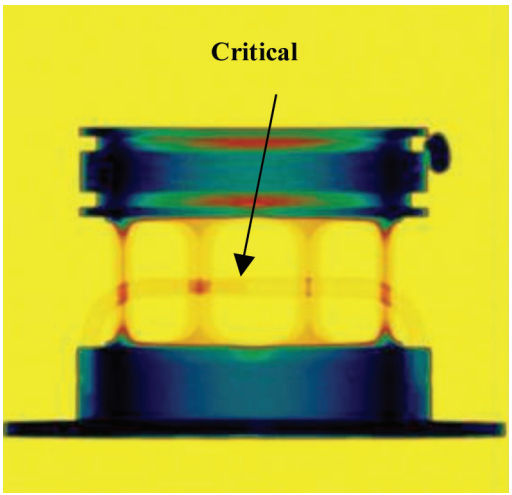

Figure 12—(b) A neutron radiograph (2-D image) of a stainless steel helicopter engine lubricator with pseudo colours defining areas of varied attenuation of neutrons

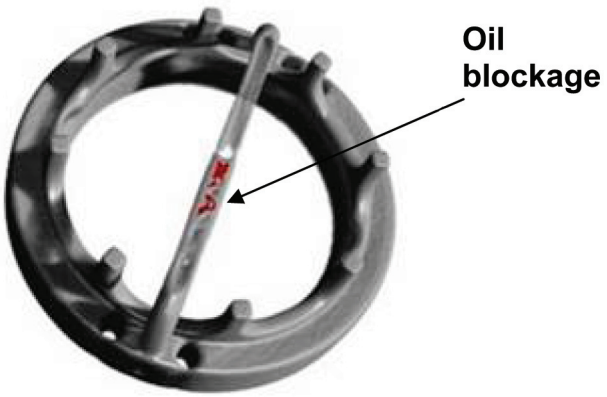

Figure 12—(d) A cutted into neutron tomogram of a of a helicopter engine lubricator revealing the blockage

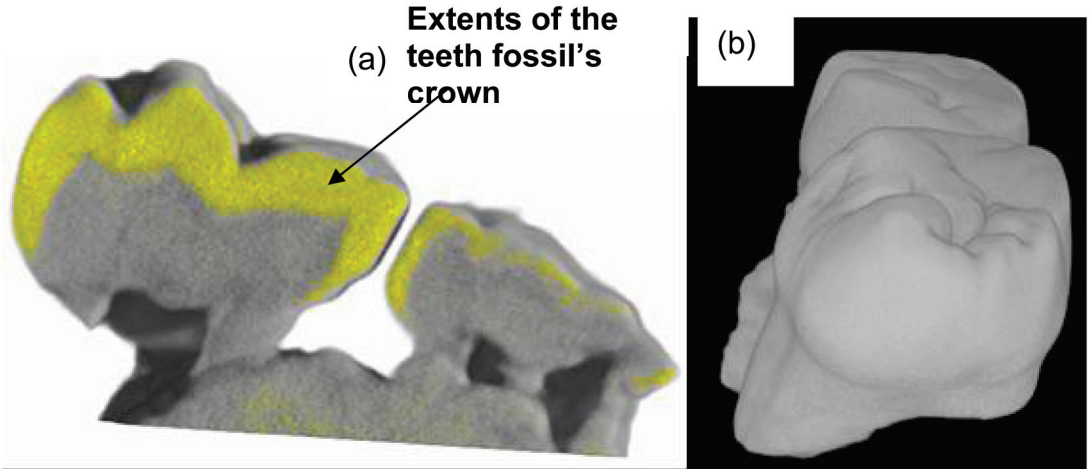

Figure 13—X-ray tomograms of teeth fossils showing its morphology

engineered model of the lubricator to enable determination of inner dimensions non-destructively. The important feature in this image is the ability to cut electronically into the sample without having to physically cut into the sample; this way one can study the internal properties of high atomic number materials.

Palaeontology: fossils

X-ray tomography has been used to obtain virtual data that can be used for morphological investigation on the set of fossilized teeth ((1.0 cm × 1.0 cm × 3.0 cm) per tooth fossil) for anatomical purposes (Figure 13). The preservation of these precious samples requires that original samples do not get to be physically handled for prolonged and repeated instances as investigation is conducted, but rather that virtual data be created for non-invasive electronical investigations on samples. X-rays were used because of the relatively finer resolution (much finer details could be achieved), compared to neutrons, and because of easy penetration. Digital tomograms make it possible to obtain data of contours and fine details from the samples and allow quantitative classification of teeth due to their structural morphology. Viewing of other important imbedded information about the teeth also becomes possible, as shown in Figure 13(a).

References

1. Bayon, G., Domanus, J. C., Greim, L., Harms, A.A., Leeflang, H.P., Markgraf, J.F.W., Matfield, R. and Taylor, D.J. *Practical Neutron Radiography*. Domanus, J. C. (ed.). Kluwer Academic Publishers, Dordrecht/Boston/London, 1992. p. 1–6.
2. Vlassenbroeck, J., Dierick, M., Masschaele, B., Cnudde, V., Van Hoorebeke, L. and Jacobs, P. Software tools for quantification of X-ray microtomography. *Nucl. Instr. Meth. Phys. Res, Accelerators Spectrometers Detectors and Associated Equipment*. A580, 2007, pp. 442–445. DOI: 10.1016/j.nima.2007.05.073
3. 3D volume rendering software VGStudio by Volume Graphics, Heidelberg, Germany. (http://www.volumegraphics.com).
4. Barton, J.P. and Von der Hardt, P. Neutron Radiography, (*Proceedings of the First World Conference*, San Diego, Califonia, U.S.A. Barton, D. Reidel Publishing Company, Dordrecht/Boston/ London. 1983.
5. Barton, J.P., Farny, G., Person, J. and Rottger, H. Neutron Radiography, (*Proceedings of the Second World Conference*, Paris, France. D. Reidel Publishing Company, Dordrecht/Boston/Lancaster/Tokyo. 1987.
6. Fujine, S., kanda, K., Matsumoto, G. and Barton, J.P. Neutron Radiography, (*Proceedings of the Third World Conference*, Osaka, Japan. Kluwer Academic Publishers, Dordrecht/Boston/London. 1990.
7. Barton, J.P. Neutron Radiography, (*Proceedings of the Fourth World Conference*, San Francisco, California, USA. Barton. Gordon and Breach Science Publishers, USA/Switzerland/Australia/Belgium/France/ Germany/Great Britain/India/Japan/Malaysia/Netherlands/Russia/ Singapore.
8. Fujine, S., Kobayashi, H. and Kanda, K. Neutron Radiography, *Proceedings of the Sixth World Conference*, Osaka, Japan. Gordon and Breach Science Publishers, Luxemburg/Switzerland/Australia Canada/France/Germany/ India/Japan/Malaysia/Netherlands/Russia/Singapore. 2001.
9. Chirco, P. and Rosa, R. Neutron Radiography, (*Proceedings of the Seventh World Conference*, Rome, Italy. ENEA, Italian National Agency for New Technologies, Energy and the Environment. 2005.
10. De Beer, F. C. Characteristics of the neutron /X-ray tomography system at the SANRAD facility in South Africa. *Nucl. Instr. Meth. Phys. Res*. A 542 2005, pp. 1–8.
11. http://www.andortech.com/.
12. Rivers, M. An IDL based tomography reconstruction package. (http://cars9.uchicago.edu/software/tomography. html).
13. Media Cybernetics, Image-Pro Plus. (http://www.mediacy.com).
14. http://www.appscintech.com/. ◆